This project has received funding from the European Union's Horizon 2020 research and innovation programme under grant agreement No 871813.

ICT Project No 871813

MUNDFAB

Modeling Unconventional Nanoscaled Device FABrication

D2.2: Atomistic catalogue of events for calibration of LKMC dedicated to silicidation and first batch of experimental results on silicidation of Si bulk materials

A. Hemeryck (CNRS), C.A. Jara Donoso (CNRS),
J. Lam (CNRS), A. Jay (CNRS), G. Landa (CNRS),
G. Larrieu (CNRS), J. Muller (CNRS), A. La Magna
A. Alberti (CNR), I. Deretzis (CNR), G. Fisicaro (CNR)

August 31, 2021

Quality management

This deliverable was reviewed by:

Peter Pichler, Fraunhofer

Anne-Sophie Royet, CEA

Contents

Executive Summary

This document reports the first set of joined theoretical and experimental investigations aiming at understanding and modelling, at atomistic resolution, the kinetics of the Ni silicidation. A combined strategy has been implemented based on: a) ab-initio energetic calculations spanning a broad set of metastable configurations for the Ni-Si system, b) ad hoc in situ experiments implementing a protocol where structural analyses are performed between two subsequent annealing steps with increasing temperatures. In addition to these investigations of fundamental character we also present some preliminary results obtained with the Multi Structures Kinetic Monte Carlo scheme (integrable in the MulSKIPS code, see also Deliverable D2.3) with the scope of demonstrating that, when suitably calibrated, this approach should be able to simulate the complex Ni-Si material modifications over the time scale of the experiments. A consistent scenario emerges from ab-initio results and first experimental data indicating a strong reactivity of the Ni/Si and Ni-rich-silicide/Si interfaces and the tendency to atomic mixing already in the as deposited samples. In addition, related to these features, a clear indication emerges for the ab-initio calibration strategy; whereas the sequential exploration of the atomistic catalogue could be more effective if dedicated to the development of Ni-Si machine learning potential (or KMC energy model) rather to be directly integrated in kinetic approaches.

1. Introduction

Contrarily to the other researches in the MUNDFAB project, the Task 2.3 activity started only after the approval of an amendment aiming at the refocus of the objectives towards the Ni based silicides materials. This request was motivated by the manufacturing flow reported in Deliverable D6.1, which indicates the Ni-silicidation as the process of interest for the contact formation in the “demonstrator” devices. The change of the system of interest has neither modified the planned investigations’ strategy nor the complexity of the T2.3 challenges since, as the Ti-Si one, the Ni-Si binary system is characterized by the stability of several compounds with different crystalline structures which have their own regime of thermodynamic stability for fixed ranges of the Ni and Si fraction and temperatures. As a consequence, the formation of the low resistivity silicide (namely the NiSi compound) can follow a complex pathway with stages dominated by other stable compounds and also intermediate structures, not present in the phase diagram. Of course, this pathway can critically depend on the preparation modality, the annealing temperature and time.

Soon after its introduction in microelectronics, continuum modelling of silicidation process appeared in the scientific literature based on calibrated coupled rate diffusion equations (see e.g. Ref. (1) for a recent development for the case of a laser-induced process). These models are able to predict the average fractions of Ni_xSi_y compounds after the process in the blanket (thin-film) configuration but, due to obvious intrinsic limitations, their formulation cannot be extended to reliably model the process in 3D nanometric structures. In order to overcome definitively these limitation in agreement with the general strategy of the MUNDFAB project, The T2.3 objective is the deep understanding of the atomistic mechanisms ruling the Ni-silicidation process and their implementation in a simulation approach with atomistic resolution which will be implemented “from the scratch”. Ideally, Molecular Dynamics (MD) appears as the correct simulation framework but the low temperatures and the duration of the process (from minute to hours) make MD application not fully feasible (it can be used only for benchmarks of ultrafast evolutions at high temperatures). As a consequence, super (augmented) Lattice Kinetic Monte (LKMC) Carlo has been indicated as the simulation scheme of reference. Of course, any LKMC model cannot be developed without a pre-assessment of the key local structural transitions promoting the kinetics, and, as indicated, this pre-assessment (which should be obtained by means of ab-initio calculations and experiments) is one of the difficult particular challenge of Task T2.3.

In the present document we will describe the first batch of ab-initio and experimental results obtained in the planned study of the Ni-silicidation process. We also add some examples of ad-hoc simulations obtained with the Multi Structures Kinetic Monte Carlo code under development for the Ni-Si systems. These early LKMC results demonstrate the necessity of a calibration strategy beyond the classical sequential study of the configuration energetics usually applied in the other applications (see e.g. Ref. (2)). We will discuss the roadmap for the future investigation identifying the Machine Learning approach as a useful strategy to overcome these difficulties.

2. Atomistic catalogue of events for calibration of LKMC dedicated to silicidation

The main task of WP2.3 is the simulation of silicide layer growth in connection with technological deposition processes. The deposition process is characterised by three steps: deposition of Nickel species on the silicon substrate, interdiffusion and reaction at the interface between the alloy phases and the silicon substrate.

In the case of silicidation, several alloy phases can be observed from Ni, Ni3Si, Ni2Si to NiSi, the latter being the phase of interest in the project. It is therefore crucial to study in detail these three stages if we want to fully reproduce the dynamics of the whole silicidation process. This requires several kinds of calculations, several strategies and new developments.

To do so, it is necessary to identify and describe the fundamental reactions during the deposition of the metallic element, here Ni, but also during the interdiffusion and reaction of Ni and Si at the interfaces between the substrate and the alloy phases. During the first months of the reference period, the calculations were carried out in order to:

- Firstly, understand the first steps of deposition by adsorption of Ni atoms on a silicon Si surface and the first insertions in the surface layers of this substrate, until the formation of a native alloy.
- In a second step, based on these observations and possible developments in the KMC, we studied systems with already built interfaces to understand the interdiffusion and reaction mechanisms to calibrate the LKMC code.

2.1 Thorough study for the understanding of the first stage of deposition and interdiffusion

2.1.1 Deposition and Ni insertion

The aim of this first study is to get an idea of the interfacial zone formed spontaneously in the early stages of silicide elaboration during the deposition of Ni on Si. A two steps approach is conducted: first the adsorption of Ni atom on the Si surface is studied and then from the most favorable adsorbed positions, we study the Ni insertion mechanism in the Si substrate. In addition, the effect of an increasing coverage of Ni is also addressed by progressively adsorbing increasing number of Ni atoms on a clean reconstructed Si surface (2x1).

Details of calculations – The modelled surface is a (2x1) reconstructed (100) surface. The deposition consists in studying the adsorption of the nickel atom above the surface as a function of the topology of the reconstructed Si surface. Our supercell is made of 272 atoms, which correspond to 16 layers of Si and 32 atoms of H located at the bottom layer for the passivation of the dangling bonds. 15 Å of vacuum is added above the topmost layer to introduce surface effects, the surface exhibits eight Si-Si dimers organized as two rows of four dimers separated by a channel. Calculations have been performed by means of the density functional theory (DFT) implemented in the Quantum ESPRESSO simulation Package (3) The Perdew–Burke–Ernzerhof (PBE) generalized gradient approximation of the exchange and correlation functional (4) within its Projected Augmented Waves pseudo-potentials (PAW) have been used (5). An energy cutoff of 50 Ry has been chosen for wavefunctions to ensure a total energy convergence of 10^{-4} Ry. The sampling of the Brillouin zone was performed at the

Gamma point. Activation barriers have been determined using the refine saddle mode of ARTn/QE coupling (6),

Ni adsorption on Si substrate - To study the deposition process, we first identify the Ni adsorption sites on Si. All tested configurations are shown in Figure 1. The most favorable positions for the first steps of the deposition have been identified: All these sites are located above the dimer row between two dimers (DB (DimerBed) and MD (Middle) configurations in Figure 1.b) and c) respectively), and above the channel (DC (DeposedChannel) and CB (ChannelBridge) configurations in Figure 1.a) and d) respectively).

Ni diffusion on Si surface - After the identification of the most favorable sites for the adsorption of Ni on the Si, we study the diffusivity of the Ni atom on the Si(100)-(2x1) surface (Table 1). We observe that MD configuration can diffuse easily toward DB configuration, and atoms in CB configuration will result as DC configurations, both with small activation barriers (~0.1 eV). Activation barriers of back reactions are larger than 0.3 eV (respectively 0.315 eV and 0.558 eV).

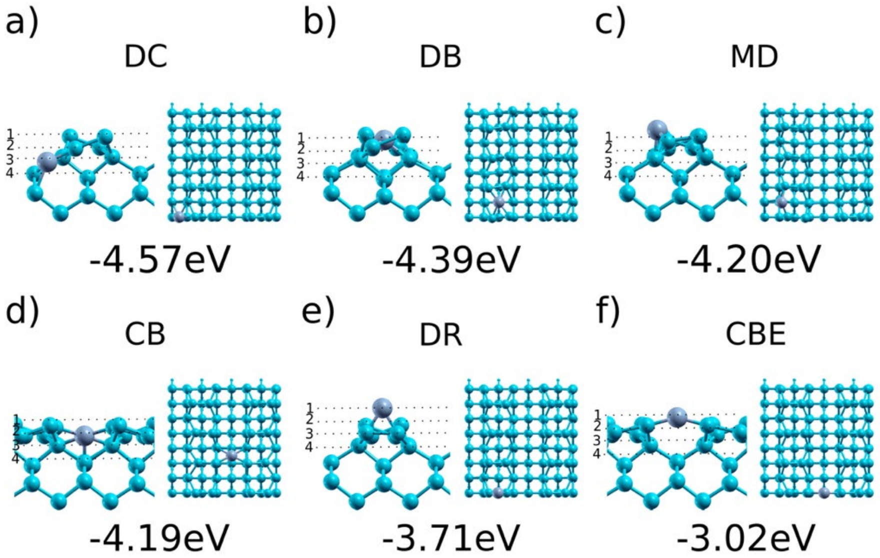

Figure 1. Adsorbed Ni configurations with their corresponding adsorption energies in eV. a) DeposedChannel (DC) consists in one Ni atom on the channel between the third and fourth layer, b) DimerBed (DB) where the Ni atom is situated between two Si-Si dimers of the same row, c) similarly in Middle (MD) the Ni atom is situated between two Si atoms of adjacent dimers in the same row, d) ChannelBridge (CB) consists in one Ni atom deposed in the channel between the second and third layer and equidistant to two dimers of different rows, e) DimerRow (DR) consists in one Ni atom deposed centered above a Si-Si dimer, f) ChannelBed (CBE) consists in one Ni atom between two dimers of different rows, situated above of the first layer. Blue and grey spheres correspond to silicon and nickel atoms respectively.

Table 1. Ni diffusion on the Si surface. The letters of the configurations refer to the Figure 1.

Configurations	c) → b)	b) → c)	c) → d)	d) → c)
Act. Barrier (eV)	0.117	0.315	0.513	0.509

Configurations	d) → a)	a) → d)	c) → a)	a) → c)
Act. Barrier (eV)	0.182	0.558	0.525	0.899

From adsorption and surface deposition steps, we conclude that:

> - DB (Dimer Bed) configuration (b) on Figure 1 which consists of one Ni atom situated on the dimer row between two dimers,
>
> - DC (Deposed Channel) configuration which consists of one Ni atom inserted in a Si-Si bond in the channel (a) on Figure 1

are the most likely configurations on the Si surface.

Ni insertion on Si substrate - The next step that is studied, is the mechanisms of insertion of the Ni atom into the silicon substrate. The aim of this study is to estimate the ability of Ni atoms to insert into the surface layers of the silicon substrate. This insertion step, which follows the adsorption step described above, therefore starts from the most favorable adsorption sites identified in the previous paragraph.

One Ni atom insertion - The insertion mechanisms for one Ni atom is described in Figure 2. The early deposition step is followed by the insertion of the Ni atom into the top layer of the silicon substrate due to the low activation barriers that are obtained for the insertion (accessible for deposition temperatures even at room temperature).

From DB (from left to right part of Figure 2) the activation barrier is 0.4 eV and allows an energy gain for the system of 1.3 eV. The system reaches the configuration called IDB (for Inserted Dimer Bed). However, from the IDB configuration, the insertion in the fourth layer from the surface, requires a large activation barrier of 1.2 eV and destabilizes the system by 1.3 eV. Note that in this last configuration labelled IDC for Inserted Deposited Channel configuration, the Ni atom finally reaches a 6-fold coordinated configuration.

The same insertion process is tested from the DC configuration (from the second-right structure to the left part of Figure 2) where a smaller activation barrier of 0.3 eV is obtained but the reached configuration is again IDC, and less stable by 0.1 eV.

Note also that we did not succeed to stabilize a Ni atom in the layer 5 and 6 from the top of the surface. All tested starting positions relaxed to the IDC configuration.

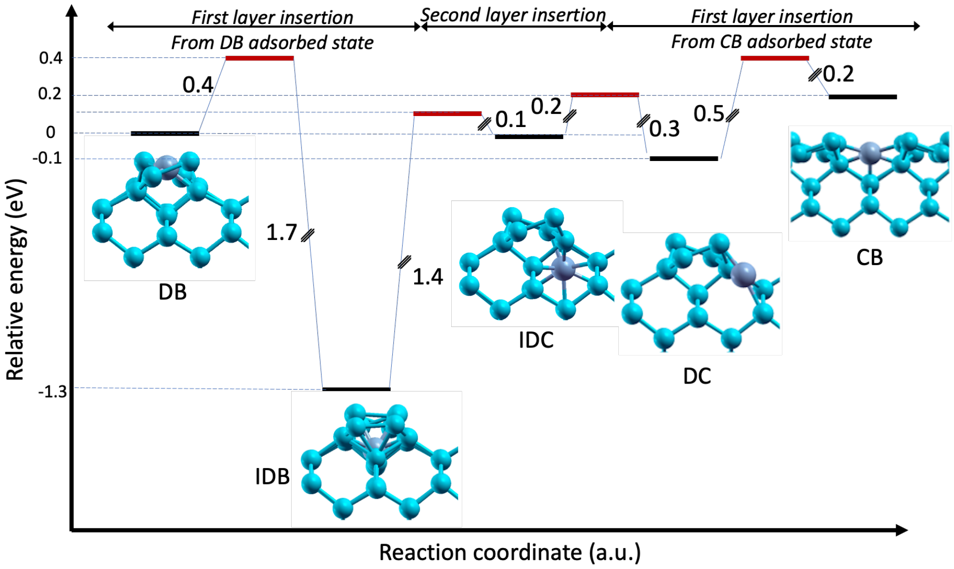

Figure 2. Insertion paths for one Ni atom into the substrate. The given energies are the activation barriers between two configurations calculated by ARTn-QE coupling (in eV).

At this low coverage level, Ni insertion is limited to the topmost layer and the IDB configuration is the favorable configuration at very low coverage.

Two Ni atoms insertion - In the case of two Ni atoms adsorbed in close proximity, both on DB configurations (Figure 3) the insertion in the fourth layer is facilitated where a decrease of the activation barrier and a stabilization of the system are observed. Note that the first insertion of one Ni atom into the Si surface layer is not affected by the presence of the second Ni atom. After the first insertion, the configuration is composed of one Ni atom in an IDB position and one Ni atom in a DB position.

From this DB/IDB configuration, two insertion paths were investigated:

- The inserted IDB atom diffuses further into a deeper layer of the Si substrate to reach an IDC position. This diffusion requires an activation barrier of 0.6 eV and does not stabilize the system (∆E = +0.1 eV).
- The atom in position DB diffuses to reach also an IDB position. This diffusion is very favorable because it is associated with an activation barrier of 0.2 eV and allows to stabilize the system considerably by 1.6 eV.

Note that from this configuration of two IDB atoms, one of the atoms diffusing to an IDC position destabilizes the system and is therefore not favorable.

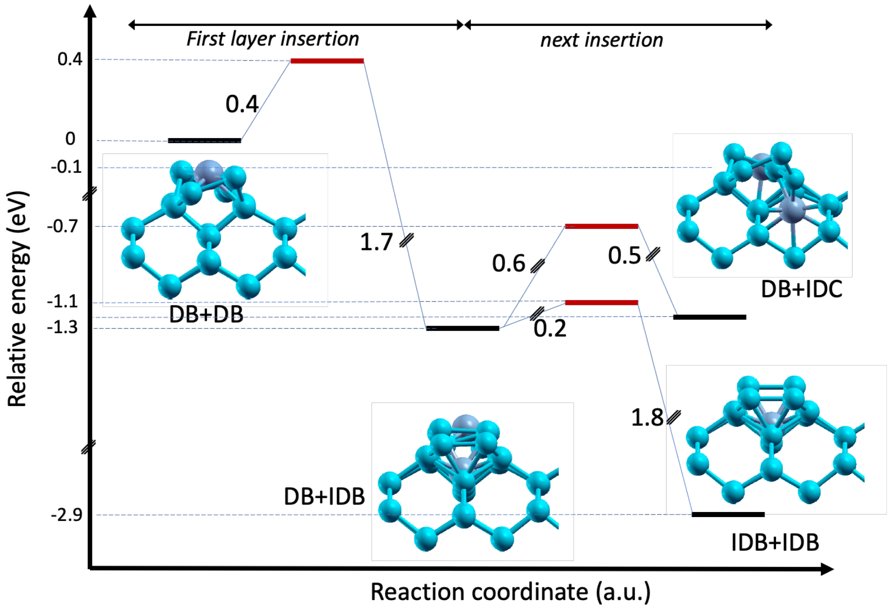

Figure 3. Insertion paths for two Ni atoms into the Si substrate. The given energies are the activation barriers between two configurations calculated by ARTn-QE coupling (in eV).

For the case of the adsorption of two Ni atoms, we also studied the influence of the presence of a Ni atom adsorbed in DB on the adsorption and insertion of a second Ni atom above the channel in its close vicinity.

We observe a spontaneous insertion of an adsorbed Ni atom into the channel toward an IDC position without any activation barrier. The presence of one already inserted Ni atom (see Figure 4 top) or more (see Figure 4 bottom) in the surface layer of the silicon thus aids in the insertion of Ni atoms into the deeper layers of the substrate.

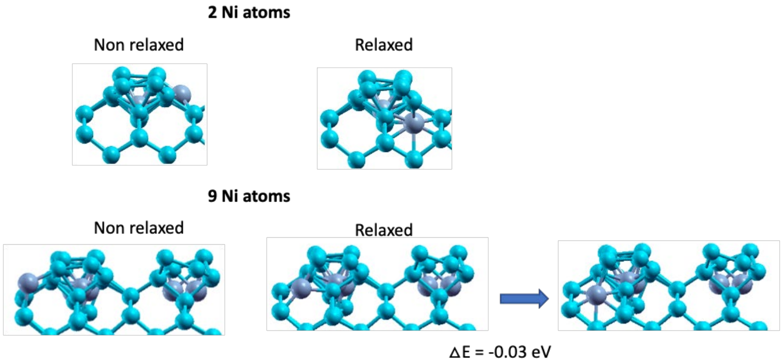

Figure 4. Relaxation of initial starting DC configuration in the presence of IDB Ni atom in close vicinity (top: 1 IDB Ni atom, bottom (8 IDB Ni atom)

We note here that it is more favorable for Ni atoms to insert into the first surface layer under the dimer row than to diffuse into a deeper layer. However, we also see that as soon as the first surface layer contains Ni atoms, the insertion in the deeper layers becomes favorable where atoms inserted below the dimer row in IDB configuration facilitates the insertion through the channel toward an IDC configuration. We note here that the DC position is not favorable until the neighboring IDB sites are filled.

The formation of the alloy on the surface of the silicon substrate seems to occur layer by layer. This trend is consistent with the rapid formation of the surface alloy as a thin layer.

The primary DFT calculations carried out step by step by adding the atoms one by one on the Si surface, demonstrate the tendency of the nickel atoms to insert themselves into the Si substrate. We then identify the stable sites in the topmost surface layers, sites that we use to build an alloy structure.

In the next section, we propose a structure and a thickness for a stable native alloy.

2.1.2 Structure of a native surface alloy

As the configuration space becomes complex and presents too many possibilities, a manual prospecting, adding one atom per atom is not feasible. We have built an alloy layer and an interface by filling all the favorable sites layer by layer. As observed in the previous part of the present report (2.1.1), Ni atoms favorably insert in IDB and IDC sites in the topmost layers of the silicon substrate. Figure 5.a shows the interface structure when all IDC are fully occupied. It is notably interesting to notice that on the Figure 5.a, the ‘NixSi’ layer formed by the addition of Ni atoms in IDC sites is similar to the ‘NixSi’ layer observed in the Ni3Si crystalline bulk. In Figure 5.b, in addition to IDC sites, IDB and CB sites are occupied. CB sites are stabilized when IDC sites are occupied. Such coverage allows also to obtain a ‘NixSi’ layer. Ni3Si can be easily adapted from the Si crystalline lattice when inserting Ni between the Si atom on the surface and in between Si layers (Figure 5.c and Figure 5.d), thanks to the close fitting of lattice parameters of the Ni3Si crystal in the [100] direction and of the Si crystal in the [110] direction (Figure 6) (respectively 3.505 Å vs. 3.83 Å).

This process leads us to the coherent formation of a Ni3Si type alloy on the surface of the silicon substrate. This finding is consistent with the experimental data (see experimental results provided in section 3). Additional calculations are under progress to fully explain the Ni3Si formation, notably about the formation of the *‘pure Ni layer’* observed in the Ni3Si alloy.

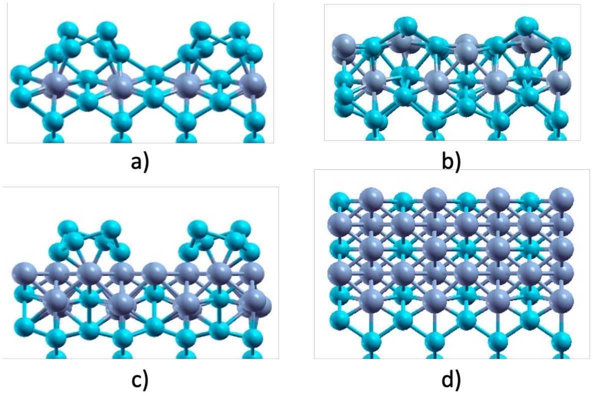

Figure 5. Side-views of the step-by-step construction of the surface Ni3Si alloy on top of Si substrate a) all occupied IDC sites b) full IDB-IDC configuration, c) a pure Ni layer is stabilized above an all-occupied IDC configuration, d) Structure and minimal thickness of Ni3Si alloy as deposited on Si substrate.

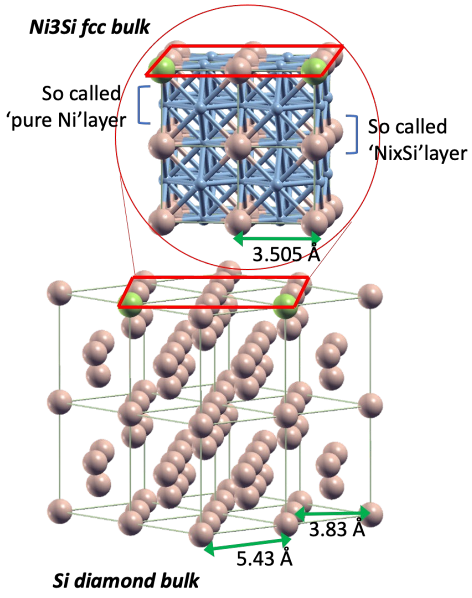

Figure 6. 2x2x2 Unit cells of Ni3 fcc Si bulk (top) and Si diamond bulk (bottom) where the similarities between the two crystals are highlighted in coherence with the formation of the native alloy formed during the deposition of Ni on Si.

From this thorough DFT study, two interfaces have been assumed for the calibration of the LKMC code, as starting systems: a Ni/Si interface without formation of an interface alloy and a Ni3Si/Si interface assuming the formation of an interface alloy due to intermixing diffusion from the first moments of deposition. Calibration is detailed in the following.

2.2 Calibration strategy for the LKMC code

The calibration of the LKMC, as will be described in detail later in this report, requires an exhaustive description of up to 32 different local environments for each of the systems likely to be encountered. As systems likely to be encountered, we must consider here bulk systems such as Si, Ni, Ni3Si, Ni2Si, NiSi, but also systems with various interfaces, such as Ni/Si, Ni3Si/Si, Ni2Si/Si, NiSi/Si but also Ni3Si/Ni2Si etc.

The calibration of the LKMC is done by exchanges of atoms in the systems listed above. Since the beginning of the project, we have been working on the systems as suggested by the DFT, *i.e.,* Si, Ni3Si, and Ni/Si and Ni3Si/Si. At first, only the configuration energies have been determined. The DFT calculations we have done for these systems are presented below.

2.2.1 Calibration on Ni3Si bulk exchanges

In Ni3Si bulk, the local atomic environment for the first exchanges authorizes only exchanges between Si and Ni atoms and implies only two possibilities: One exchange in 'NixSi' layers by inverting one Si atom with one Ni atom in the same layer (struct 1 on Figure 7 left) and one exchange between the 'NixSi layer' and the 'pure Ni' layer where one Si atom of the 'NixSi' layer is inverted with a Ni atom of a 'pure Ni' layer (struct 2 on Figure 7 right).

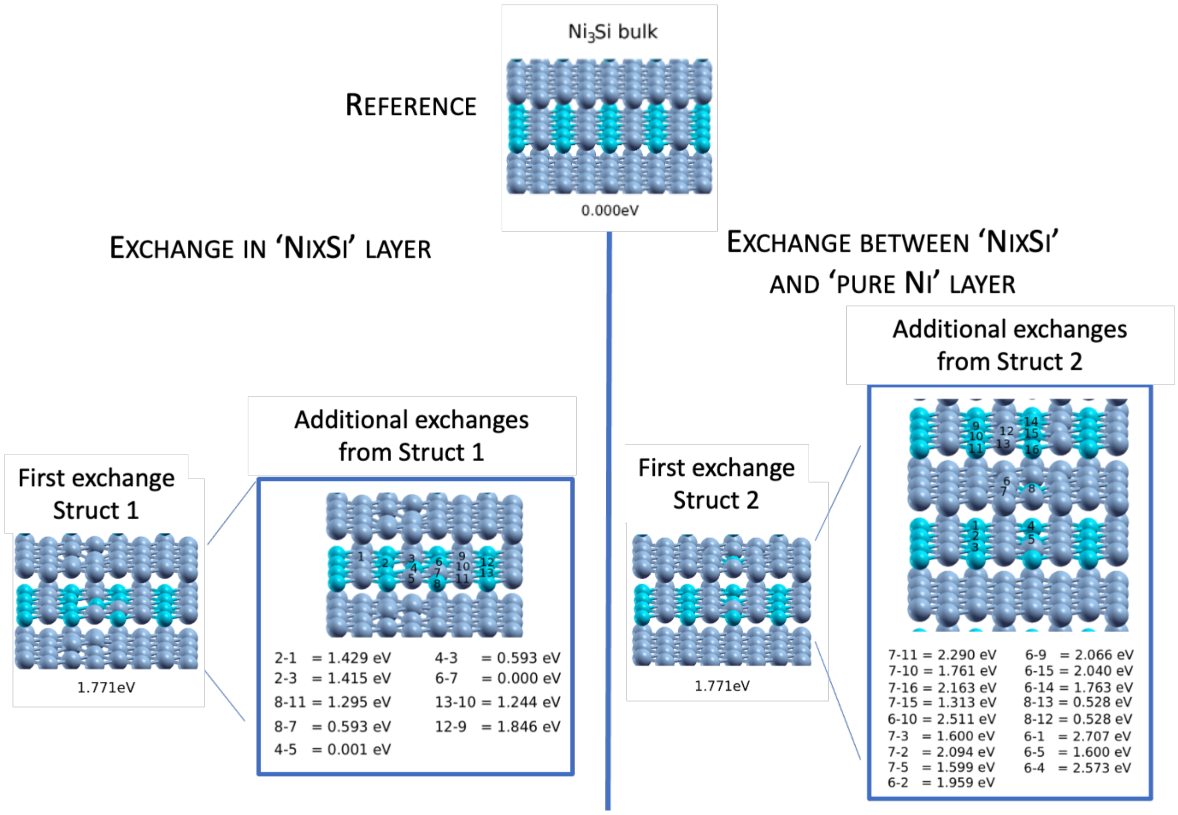

Figure 7. Calibration strategy for the LKMC using DFT calculations in Ni3Si bulk. Left: exchanges in 'NixSi' layer by inverting one Si atom with one Ni atom in the same layer. Right: exchanges between the 'NixSi layer' and the 'pure Ni' layer where one Si atom of the 'NixSi' layer is inverted with a Ni atom of a 'pure Ni' layer. The energy differences are given, with reference to the bulk system. The vertical axis has been enlarged for better visualization.

Logically, such exchanges are not favorable, consistently with the well-organized formation of crystalline alloys, characterized by an energy difference in respect to the perfect Ni3Si bulk of 1.771 eV in both cases. Then, additional exchanges are applied from struct 1 and struct 2. However, exchanges within the same layer are in general more favorable than exchanges between layers (two exchanges from structure 1 have energy differences close to 0). We also observe that the exchange of atoms close to the previously exchanged atoms is more favorable than the exchange of distant atoms.

From the calculated additional exchanges, it is then obvious that many more exchanges can be applied. This was the initial strategy considered in this work, but in view of the large number of different configurations then possible, it becomes obvious that such a strategy is difficult to maintain.

2.2.2 Calibration on systems with interfaces

In this section we discuss the strategy chosen to model interface systems, which will be used for the calibration of the KMC.

For the interface modelling, we bring together the two slab systems we aim to study. The host substrate is silicon as used experimentally, on which we position the nickel slab or the alloy slab. The lattice parameter of the nickel slab and the alloy slab are both adapted to match the parameter of the silicon slab by considering that the substrate imposes its stress on the deposited material.

To start the interface modelling, we consider the case of a Ni/Si interface without formation of an interface alloy and the case where the Ni3Si/Si alloy was formed at the first instants of deposition in connection with the previous observations. The lattice parameter of silicon is 5.43 Å, the lattice parameter of nickel is 3.53 Å, and the lattice parameter of Ni3Si alloy is 3.505 Å. Respectively for the [110] and 2 x [100] directions a lattice mismatch of 8 % is obtained (consistent with the use of the same lattice in the KMC).

- DFT simulation cell of the NiSi/Si interface: An equivalent to two-unit cells thick layer (i.e. 5 Ni atomic layers thick) slab is directly put in contact with the silicon reconstructed surface, with the Ni lattice parameter modified to adapt to the Si one. The Si substrate is the same as described previously for the adsorption study. After minimization, the Ni layers are not affected by the presence of the interface with silicon, the Ni remaining in a crystalline configuration (Figure 8 a/). This model interface is therefore consistent with a calibration strategy for the LKMC.
- DFT simulation cell of the Ni3Si/Si interface: A five Ni3Si layers thick slab is directly put in contact with the silicon reconstructed surface, with the Ni3Si lattice parameter modified to adapt to the Si one. The Si substrate is still the same as described previously for the adsorption study. In this case, when the assembly of the two materials is relaxed to exhibit a common interface, we observe a distortion of the Ni3Si slab in contact with the silicon. It becomes very difficult to identify positions such as on lattice. It should also be noted that experimentally an additional thick layer of Ni is deposited and is present above the Ni3Si substrate imposing a bulk effect on this material. In this work we must also agree on a reasonable computation time for the DFT calculations to be performed. Thus, we have carried out tests of the interface models presented hereafter fixing in turn layers in full or partially.

2.2.2.1 Calibration on Ni/Si interface exchanges

For the case of the Ni/Si interface, the reference system shows a crystalline structure for the Ni layers (Figure 8 a/) and is featured by a reconstruction at the interface between the two materials that mimics the dimers of the (100) Si surface.

From this system, the only first exchange we can apply is an exchange between a Si atom and a Ni atom directly between the layers at the interface between the two materials. This exchange (Figure 8.b/) is highly favorable with an energy gain of -1.33 eV. This shows the favorable tendency to the formation of a silicide type alloy when the two materials are brought into contact.

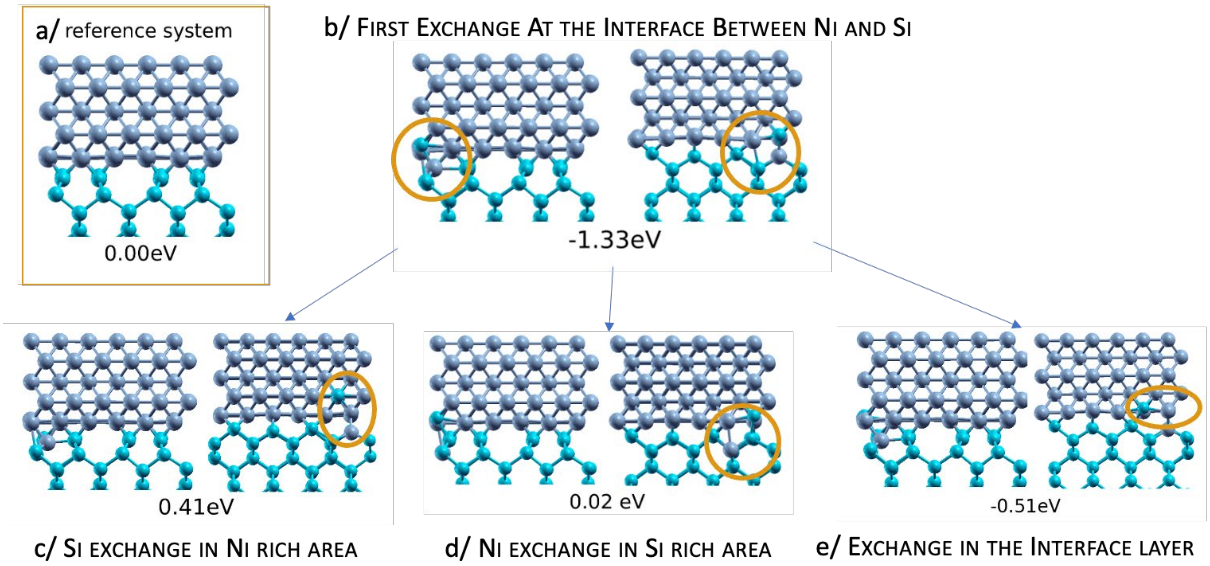

Figure 8. Calibration strategy for the LKMC using DFT calculations in NiSi/Si interface system. a/ Ni/Si interface reference system. b/ first exchange at the interface. c/ d/ e/ additional exchanges between Si and Ni atoms from the configuration b/. Relative energy of b is determined in respect to a/ reference system. Relative energies of c/ d/ and e/ are determined in to respect b/ configuration. b/-e./ two side views and orange circles are used to help the visualization of the exchange zones.

Then, from this exchange, additional exchanges are performed around the modified local configuration in order to increase the sampling of the space of local configurations. Several cases are thus tested in the adjacent layers in materials richer in either Si or Ni, i.e., further from the interface (Figure 8 c/ and d/) and at the interface (Figure 8 e/). A positive energy difference of 0.02 eV is obtained for exchange toward deeper Si layers (in rich Si area) and 0.41 eV is obtained for exchange toward Ni bulk (in rich Ni area). At the opposite, an energy gain is obtained when an exchange in the interface layer is carried out.

Here we show that diffusion at the direct interface between Ni and Si materials is the favorable mechanism for the intermixing zone. We see those diffusions of both Ni and Si into Si and Ni rich zones are not favored at the concentrations tested. This trend is consistent with the formation of a spatially limited alloyed zone driven by atomic exchanges at the interfaces.

2.2.2.2 Calibration on Ni3Si/Si interface exchanges

For the case of the Ni3Si/Si interface, different approaches can be taken (Figure 9), the different approaches will have sense depending of different experimental frames depending for instance of the deposition parameters. This choice is also motivated in the scope of the LKMC development, where the feature on Lattice requires a localization on a 3D point of the atoms. We consider in the following notably a full relaxation which mimics the freedom of all the atoms of the structure to move, the three Ni3Si top layers completely fixed, one Ni3Si top layer completely fixed, and one Ni3Si top layer fixed in the horizontal plane but free in the perpendicular plane.

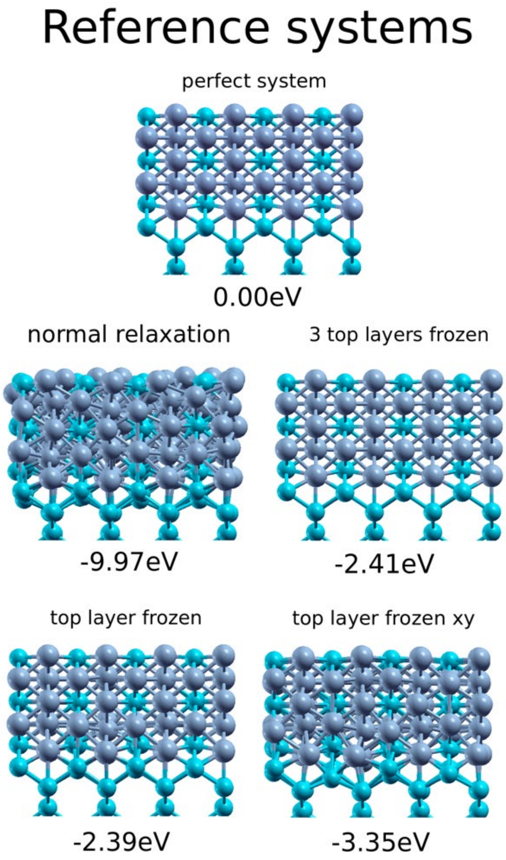

Figure 9. Different simulation approaches for the Ni3Si/Si interface systems investigated. These approaches differ in the way the upper layers of the Ni3Si material are relaxed or not.

It is particularly interesting to observe that for a case such as a thin layer of Ni3Si deposited on the surface (the Normal relaxation case in the Figure 9) we observe a material of Ni3Si composition but whose structure is not well defined, in the sense that the atoms in this zone are not perfectly localized on the crystalline bulk positions. This modeled case could be assimilated to a low coverage of deposited Ni, or a low flux. As soon as we introduce a constraint (more or less strong) in our Ni3Si layer during the relaxation, the material keeps its stoichiometry but also its crystalline-like structure. This modeled case could correspond to a Ni material deposited in large quantity and leading to a relaxation stress in the Ni3Si material in contact with. Unfortunately, due to the limitations of DFT calculations and the sizes that can be used, it does not seem possible to model a more complex Si/Ni3Si interface, which seems to be the most realistic system to model. A strategy using a Machine Learning potential is under development, allowing to fill this lack.

Taking in account these different approaches, exchanges in the interface are made. For obvious reasons, we use for the calibration on this system an interface with a constraint in the layer to match the needs of the LKMC. In the following, we do not discuss all cases in detail, we provide only one trend on “frozen top layer” system for typical exchanges described as interfacial interlayer or intralayer. Final atomic configurations are given as side-views of the Ni3Si/Si interface in Figure 10.

We notice in particular that the so-called interlayer diffusions are the most favorable (Figure 10 b/ and c/), at least from a thermodynamic point of view. By exchange of atoms at the interface, we see that the system still gains in energy, whatever the exchange, with a more favorable tendency for the interlayer exchanges.

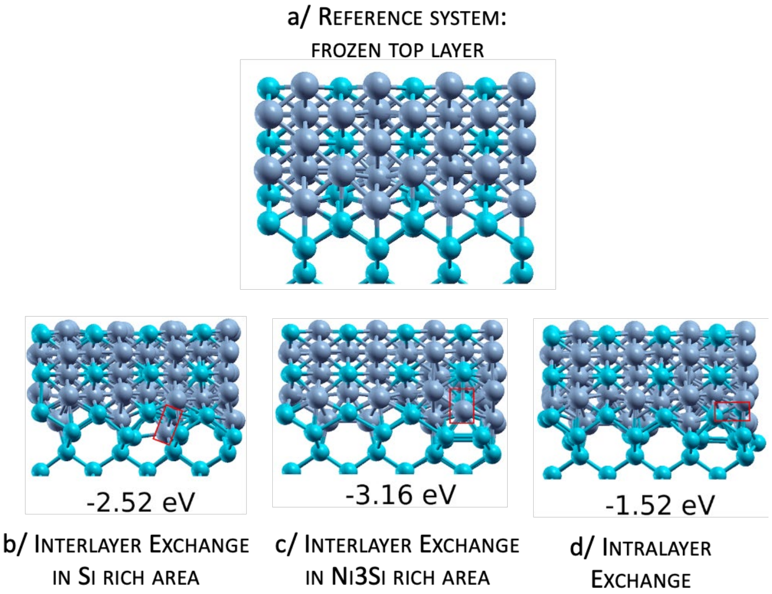

a/ REFERENCE SYSTEM: FROZEN TOP LAYER

b/ INTERLAYER EXCHANGE IN SI RICH AREA

c/ INTERLAYER EXCHANGE IN NI3SI RICH AREA

d/ INTRALAYER EXCHANGE

Figure 10. Calibration strategy for the LKMC using DFT calculations in Ni3Si/Si interface system. Some exchanges are shown on the frozen top layer system (a/) for interlayer exchange on Si-rich interface (b/), for interlayer exchange on Ni3Si-rich interface (c/), and for intralayer exchange at the interface (d/). Relative energies are provided in respect to reference system in a/.

We demonstrate here again that an exhaustive calibration in this kind of complex interface is something not bearable, not thinkable given the set of possible configurations that we have to consider. It is then necessary to think of another way to proceed, in particular by turning to algorithms of the machine learning type for a more efficient and more systematic calibration. This work has started with the development of a new interatomic Machine Learning potential based on ab initio data. The start of this work is described in the perspectives part of this report, Section 2.5.

At this stage, we are still within the limits of the DFT. To continue in DFT on the study of these interfaces for the understanding of the growth mechanisms is not possible. In the coming months, it could become necessary (if the need of going in more details on growth mechanisms appears) to change scale and methodology in particular thanks to the use of molecular dynamics.

2.3 KsLMC approach to the multi structures evolution in a silicidation process

The final scope of the kinetic simulation code for the Ni silicide formation is simulating the sequence of structural transitions from an initially prepared metal-semiconductor interface as a function of the thermal budget (temperature + annealing time). Difficult challenges for the simulations are: a) long simulated time (≈h), b) atomistic description of the crystalline structure of the Ni, Si and many Ni-Si compounds and c) mesoscopic dimension of the simulation box (≈ 100 nm is a suitable scale realistic systems).

The formalism of the Kinetic super Lattice Monte Carlo (KsLMC) method developed and implemented for the kinetic simulation is described in the deliverable D2.3. The design of the algorithm structure is strongly driven by the requirement of model flexibility in order to avoid major code modifications if a reconsideration of the kinetic scheme is necessary. In the current scheme the reference super-lattice is a simple cubic one with a lattice constant $a_{SL}= a_{Si} /12$ where a_{Si} =0.543 nm is the Si conventional cubic lattice constant.

In this super-lattice we correctly map the Si diamond crystal and with a very good approximation the pure Ni and Ni_3Si close packed structures. For example, we have that

- Possible Si-Si next neighbor atoms of the site (0, 0, 0) are ($3a_{SL}$, $3a_{SL}$, $3a_{SL}$) ($-3a_{SL}$, $-3a_{SL}$, $3a_{SL}$) ($3a_{SL}$, $-3a_{SL}$, $-3a_{SL}$) ($-3a_{SL}$, $3a_{SL}$, $-3a_{SL}$)
- Ni-Ni fcc next neighbor atoms of the site (0,0,0) are e.g. ($\pm 4a_{SL}$, $\pm 4a_{SL}$, 0), ($\pm 4a_{SL}$, 0, $\pm 4a_{SL}$) (0, $\pm 4a_{SL}$, $\pm 4a_{SL}$)

The four Si next neighbors are particular positions of the 32 sites in the 27th neighbors shell of the superlattice (see e.g., Table 2), whilst the Ni-Ni next neighbors are all the 12 sites of the 32th neighbors shell of the superlattice.

Table 2. Integer coordinate of the 27th shell of neighbors in the reference super-lattice. Four possible tetrahedrally configurated neighbors (i.e., ideal Si bonding network) with respect to the origin are marked in yellow.

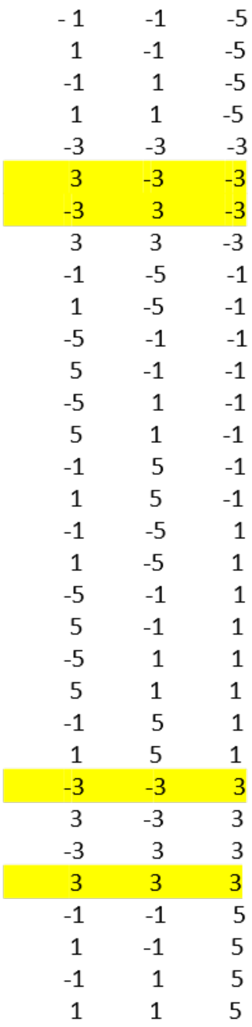

- 1	-1	-5
1	-1	-5
-1	1	-5
1	1	-5
-3	-3	-3
3	-3	-3
-3	3	-3
3	3	-3
-1	-5	-1
1	-5	-1
-5	-1	-1
5	-1	-1
-5	1	-1
5	1	-1
-1	5	-1
1	5	-1
-1	-5	1
1	-5	1
-5	-1	1
5	-1	1
-5	1	1
5	1	1
-1	5	1
1	5	1
-3	-3	3
3	-3	3
-3	3	3
3	3	3
-1	-1	5
1	-1	5
-1	1	5
1	1	5

As an example of crystal mapping in the super lattice, the MulSKIPS output for the Ni_3Si-Si and Ni-Si perfectly epitaxial interface is shown in Figure 11. Of course, substitutional Ni-Si alloys (e.g. Si diluted density in Ni crystal) can also be mapped; moreover a reliable matching between the lattice positions for crystals of other silicides compounds (e.g. Ni_2Si, NiSi and $NiSi_2$) and a sublattice of the reference super lattice can also be attempted on the basis of the improved knowledge of the fundamental steps, including the meta-stability of intermediate configurations, which promote the overall microstructural evolution.

Strongly disordered configurations (i.e. pseudo-amorphous ones) can play a fundamental role in this complex kinetic evolution, especially as intermediate conditions which mediate the transition between different compounds/crystal structures. These amorphous configurations can naturally arise in super-lattice simulated kinetics, in this case only average fields can be used in the code calibration and validation stages.

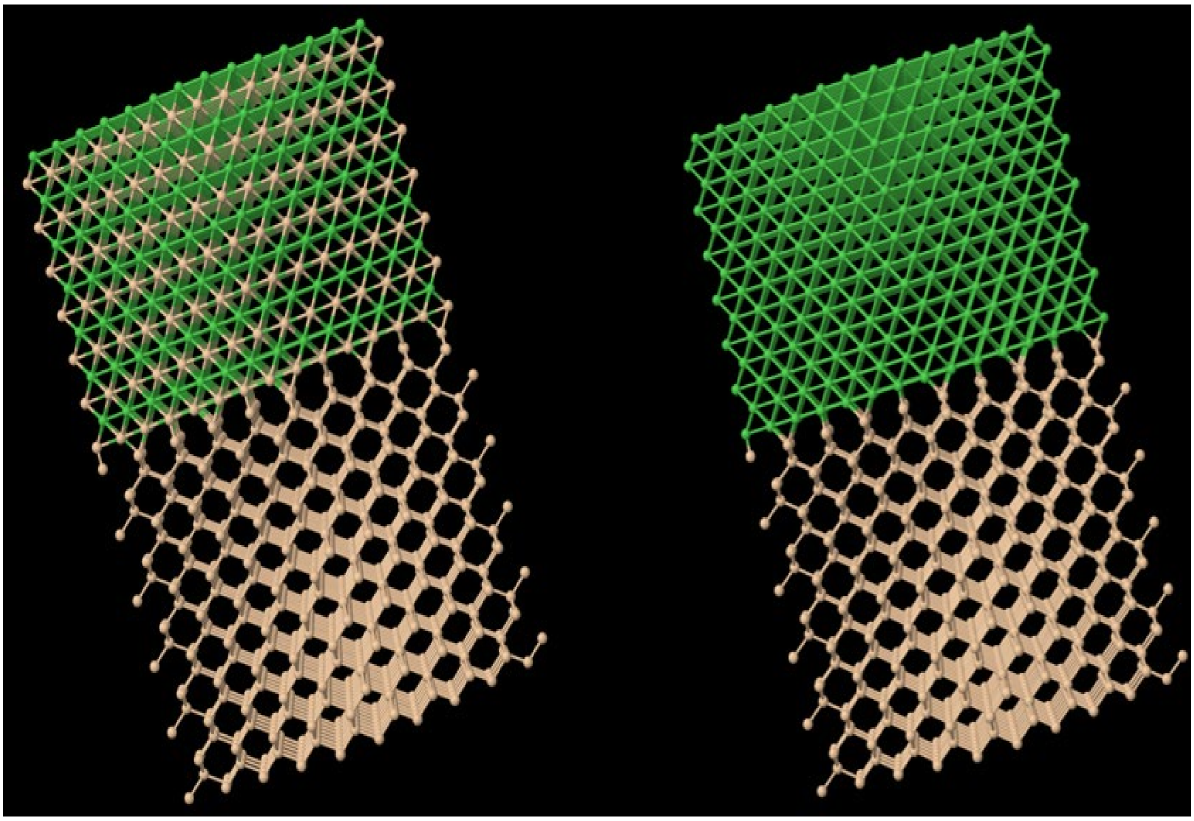

Figure 11. Ideal Ni-Si (right panel) and Ni3Si (left panel) interfaces as they are mapped in the reference super-lattice.

2.4 Example of simulations for “ad-hoc” choice of the model setting

The key of the success for this evolution stochastic model is a suitable calibration of the event frequency/configuration functional presented in the D2.3

$$\nu^{X}_{Event}\quad \left[(n_{1ho}, n_{1he,} n_{2ho}, n_{2he,} n_{3ho}, n_{3he},\ n_{4ho}, n_{4he}\dots); T\right] \qquad (1)$$

where the indexes 1,2,…run on all the possible neighbor shells while “ho” and “he” subscripts indicate homopolar (e.g. Si-Si or Ni-Ni) and heteropolar types of coordination (e.g. Si-Ni). This calibration also implies: The appropriate choice of setting of: a) maximum extension of the neighbor shells (from 1 to smax), b) the subset of active neighbor shells $\{n_{\beta ho}, n_{\beta he}\}$ for the energetic/frequency determination, c) the subset of active neighbor shells $\{n_{\gamma ho,} n_{\gamma he,}\}$ for the displacements/exchange transition events. This difficult task will be the objective of the future activity; anyway, the code has been test, for debugging purposes, for a broad choice of ad-hoc dependences of the functional (1). Here we discuss some results of these tests in order to demonstrate the code possibilities.

In Figure 12, some snapshots of simulated evolutions starting from a ≈2.7nm thick “Ni” film embedded in a “Si” matrix with periodic boundary conditions and the box size is about $5.4\times5.4\times10.8$ nm^3. In this case, four shells are used for both transition and energetic: 1st, 2nd, 27th (i.e. Si bonds), 32th (i.e. Ni-Ni bonds). A “toy” bond counting rule at T = 500 K is used which favors Si-Si bonds (0.6 eV per bond) in the 27th shell, Ni-Ni (0.1 eV per bond) and Ni-Si (0.15 eV per bond) in the 32th, while all the other bonds are not favored (between 0.01 and 0.05 eV). Of course, this choice has no claim to represent any realistic systems. Anyway: no error occurs after a long run (2×10^7 MC steps) and qualitative interesting features: strongly disordered configuration form at the original "Ni"-"Si" interface, an "NiSi" (Ni rich) alloy takes the place of the original Ni film with increasing Si content. However, the evolution destabilizes the "Si" zones indicating the complete lack of any physical meaning of the results. We have also tested whether a system similar to the alloy "Ni" region in the right panel of Figure 12 can evolve to ordered "Ni_3Si" configurations if the Ni:Si content is close to the 3:1 ratio.

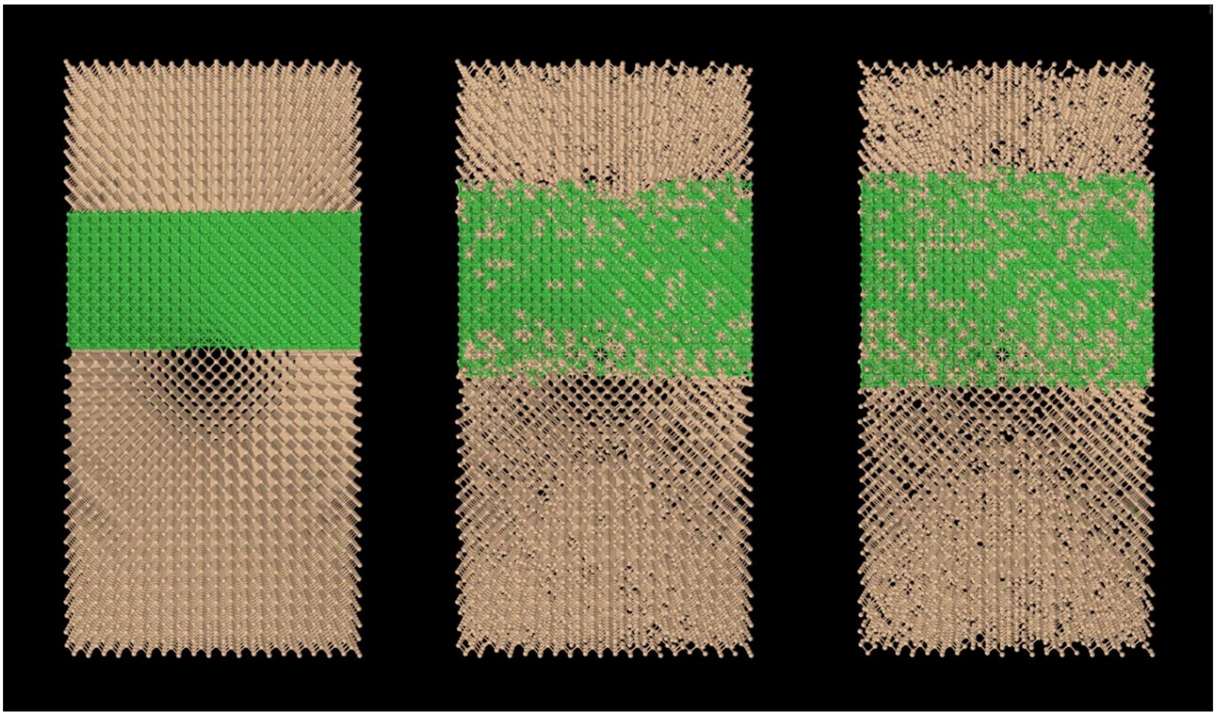

Figure 12. Snapshot of KsLMC evolution the ideal NiSi systems described in the text. Left panel initial iteration, central panel snapshot after 10^7 iterations, right panel snapshot after 2×10^7 iterations.

In Figures 13 and 14, examples of these cases are shown for the case with a completely random substitutional Si distribution in the Ni lattice and the case with an ordered Ni_3Si seed in half of the computational box. The box size is about $5.4\times5.4\times10.8$ nm^3 and the "toy" energetic choice is the same as of the case already discussed. From the graphs the formation of ordered Ni_3Si-like configurations is clear where the presence of the seed increases the epitaxial ordered, whilst small ≈nm-wide Ni_3Si regions can be observed in the case of full random choice.

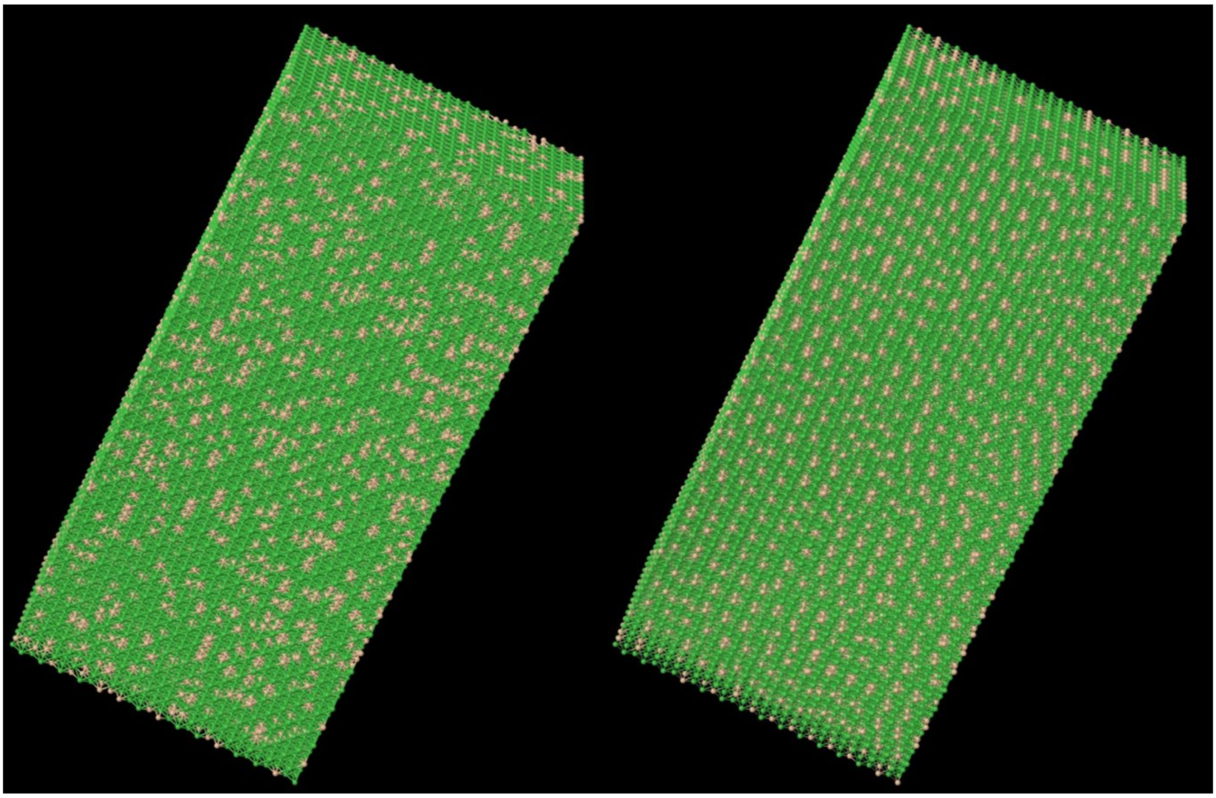

Figure 13. Snapshot of KsLMC evolution the ideal NiSi alloy with 1:3 composition described in the text. Left panel initial iteration, right panel snapshot after 2×10^7 iterations.

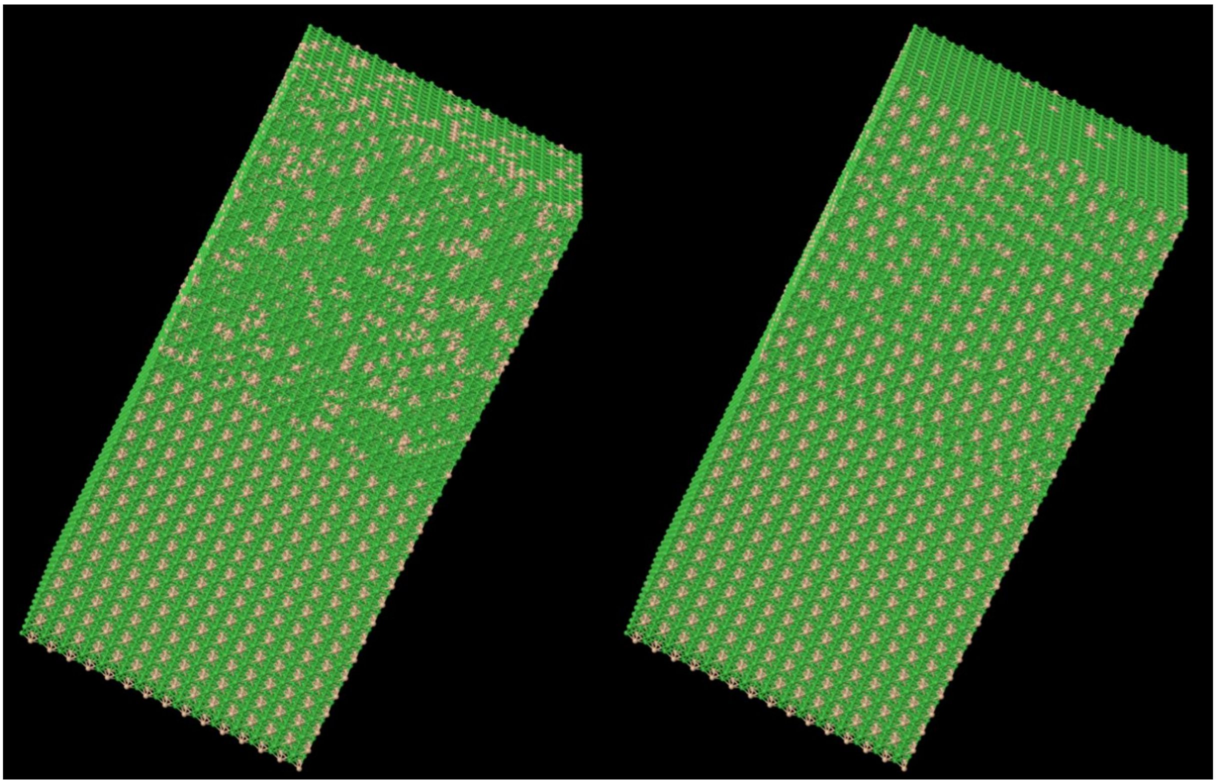

Figure 14. Snapshot of KsLMC evolution the ideal NiSi alloy with 1:3 composition described in the text with a Ni3Si seed in the bottom of the simulation box. Left panel initial iteration, right panel snapshot after 2×10^7 iterations.

2.5 Modeling perspectives: Machine Learning potential based on DFT data to match local environment in NixSiy alloys

The formation of surface alloys is a difficult phenomenon to model due to the multitude of mechanisms that can occur during formation. While DFT allows for a detailed understanding of the early stages of growth, and a description of the reaction mechanisms at the interface once the alloy is formed, its large computational cost prevents from describing large-scale mechanisms like elastic distortions and phase transformations.

In order to overcome this intrinsic limitation of DFT, one could employ classical force fields. However, for silicides, there is currently no interatomic potential that can correctly predict the geometries and properties of the many possible phases of NixSiy alloys, notably those involved in the current silicides study. The only interatomic potential is an MEAM potential that uses the Ni3Si phase as reference system (7). This potential gives us an error around of 2.75 % for the cell parameter of Ni3Si, 7.09 % for Ni2Si and 5.85 % for NiSi, and errors around of 48.47 % for the energy per atom of Ni3Si, 33.43 % for Ni2Si, and 31.40 % for NiSi.

Considering the relatively large errors that are observed for some of the studied systems, we are currently developing a Machine Learning interaction potential (MLIP) that should allow us to perform large scale simulations while retaining the accuracy of DFT calculations. With the obtained MLIP, we will be able to carry out molecular dynamics simulations up to few nanoseconds with thousands of atoms and to probe the formation mechanisms of silicides. These MD simulations will be used as a benchmark for the LKMC ones for an efficient refinement of the model calibration, whose complexity can be only roughly addressed by the current DFT study in spite of its extension, because of the immeasurable number of configurations that we have to consider in this evolving system.

We employed the machine learning method named Physical LassoLars Interaction Potential (PLIP), developed by Julien Lam from CNRS Toulouse (8). As in the other MLIP approaches, PLIP starts with a very universal analytical formulation for the force field which is then parameterized to match a database of DFT calculations made of the combination of structures and associated forces. The originality of PLIP is the combination of a physically motivated mathematical formulation for the potential and a constrained linear regression. Indeed, on the one hand, our MLIP is constructed as a linear combination of classical interactions that are divided in two-body, three-body and many-body interactions. The latter are respectively made of simple functions (Gaussian, Lorentzian, Slater-type orbitals...), explicit angular functions and embedded atom-like interactions. On the other hand, the corresponding linear coefficients that measure the preponderance of each contribution are fitted using a specific linear regression (named LassoLars) which imposes most coefficients to be exactly equal to 0 thus providing a way to simplify the final MLIP expression and to retain only the main physical nature of the interactions.

In practice, we started by constructing a database of DFT calculations related to silicides. In particular, all bulk systems of the different alloy phases were created: Si, Ni, Ni3Si, Ni2Si, NiSi. For each of them, we used the MEAM potential to perform MD simulations where the bulk systems are heated up to the melting point allowing to span several local environments ranging from ordered to disordered. Then, along the melting path, we extracted structures and computed forces using DFT calculations. A first version of the potential was obtained and gives a good description for the NixSi, Si, and Ni energies, with a relative error (respect to DFT values) of 0.02 %, 0.02 % and 0.03 %, for Ni3Si, Ni2Si, and NiSi respectively thus already far below the errors of MEAM.

We have also a relatively good description of the NixSi cell parameters. Obtaining a relative error of 6.04 %, 4.20 %, and 11.13 %, for Ni3Si, Ni2Si, and NiSi, respectively. For Si the cell parameter has a relative difference of 0.12% with respect to DFT. However, for Ni bulk the initial error was much larger (80.38%). This is due to the fact that for Ni bulk, DFT calculations included the magnetization which is not consistent with the other calculations of the database. Indeed, when excluding the Ni bulk data, we already manage to reduce the error to reach 44.57 % (Figure 15). We will improve the modeling of Ni bulk by performing additional DFT calculations without magnetization.

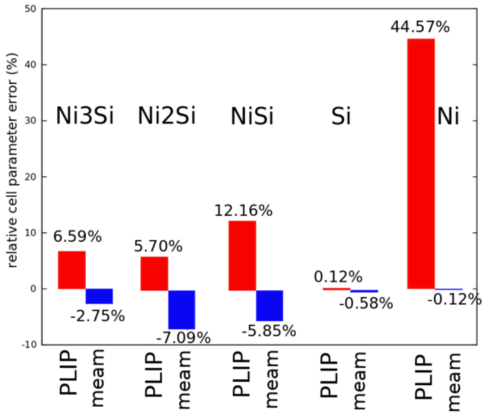

Figure 15. Relative cell parameter difference for PLIP without Ni data and MEAM with respect to DFT values

With this first MLIP, we already studied structural properties of Ni diffusion in bulk Si. In particular, we started from not relaxed structures and performed energy minimization. The structures obtained with MLIP show great agreement with DFT calculations.

As a perspective, we will improve the PLIP model using additional DFT calculations in particular those of Ni bulk without magnetization. Then, we will also test mechanical properties obtained with the MLIP model and if necessary, include more DFT calculations with distorted simulation boxes. Once the MLIP model is satisfying, we will perform MD simulations to model the phase transitions occurring at the interfaces.

3. First batch of experimental results on nickel silicides

3.1 Sample preparation

We give a detailed explanation of the fabrication process for NiSi and PtSi silicidation test samples used for X-ray and TEM analysis.

The starting wafers are 4” (100) p-Si bulk wafers, lightly doped (boron at 1×10^{15} at/cm). The wafers are firstly cleaned in Piranha (H_2SO_4:H_2O_2 1:1) solution to remove any organic residues on the surface. Secondly, the native silicon oxide layer of 1-2 nm thickness is removed by wet chemical etching in diluted hydrofluoric acid (HF(5%):Methanol 1:1) for 30s. The acid is diluted in methanol in order to follow the same process that is used for the preparation of silicon-nanowire (NW) samples which are also planned to be fabricated for WP2. Silicon-NWs have to be rinsed/etched in methanol rather than in water as its high surface tension may break the wires during the drying-process.

Then, the wafer is immediately placed under vacuum in an electron-beam evaporator “Plassys MEB-550SL” to minimize the re-formation of the native oxide layer. An optional in-situ Ar-milling is performed prior the metal deposition. The Ar plasma is obtained at a 5 sccm flow of Ar with a chamber pressure of 6.5×10^{-5} mbar for 2 min. Some test samples were fabricated without the in situ Ar milling step. The deposition of 10 nm of nickel or platinum occurs at a low deposition rate of 0.1 nm/s, at room temperature without any additional heating and with a beam power loading of 280 mA and 10 kV.

The metallized wafers are retrieved from the evaporator and stored within a N_2 locker before they are transferred. The full list of fabricated samples that have been transferred in hermetically sealed containers to the “Institute for Microelectronics and Microsystems (IMM)” for thermal annealing and characterization are listed below together with the main process parameters:

Table 3. Summary of the four deposition conditions considered for the silicidation experiments.

Sample	Si surface treatment	T deposition* (°C)	thickness (nm)	Power loading (W/cm2)	Ar milling (sccm), (mbar),(min)	A-C distance (cm)	Base pressure (Torr)
PtAr-1	1 HF5%: 1 Me 30s /rince Methanol + In situ Ar plasma	25°C	Pt 10nm	0.1 nm/s, 10kV, 280mA	5sccm 6.5.10-5 mbar 2 min	70	6×10^{-8} mbar (deposition)
Pt-1	1 HF5%: 1 Me 30s /rince Methanol	25°C	Pt 10nm	0.1 nm/s, 10kV, 280mA	no	70	6×10^{-8} mbar (deposition)
NiAr-1	1 HF5%: 1 Me 30s /rince Methanol + In situ Ar plasma	25°C	Ni 10 nm	0.1 nm/s, 10kV, 280mA	5sccm 6.5.10-5 mbar 2 min	70	6×10^{-8} mbar (deposition)
Ni-1	1 HF5%: 1 Me 30s /rince Methanol	25°C	Ni 10 nm	0.1 nm/s, 10kV, 280mA	no	70	6×10^{-8} mbar (deposition)

3.2 Structural analysis of nickel silicides

The experimental activity focuses to provide benchmark behaviors for nickel silicidation on [001] silicon substrates under specific conditions to be used for simulation calibration. For this purpose, nickel layers that are 10 nm thick were initially selected, with a further scaling of the thickness in the further course. Thermal budgets below 400 °C are targeted for silicidation. The formation of thin Ni-silicide layers at low thermal budget represents a challenge: It is accessible and applicable only if key processes are well under control such as the interdiffusion of Ni-Si species and the reaction of low resistivity phases with smooth interfaces. From what is already well known in the literature (9), a first DOI was tailored that includes as important split the status of the silicon surface before nickel deposition. A sputter etch step under Ar ions is included in sample NiAr-1 (referred to below as sputter etched, SE) with respect to the Ni-1 reference, wherein only a chemical etch is applied, as shown in Table 4. The samples, all provided by CNRS, were sent under nitrogen to preserve the nickel layer from oxidation.

Table 4: First DOI of samples

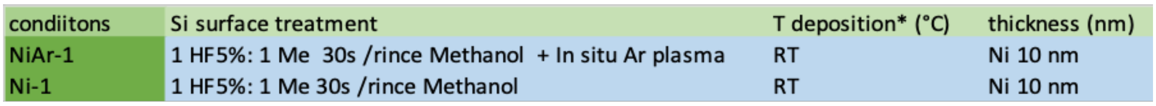

condiitons	Si surface treatment	T deposition* (°C)	thickness (nm)
NiAr-1	1 HF5%: 1 Me 30s /rince Methanol + In situ Ar plasma	RT	Ni 10 nm
Ni-1	1 HF5%: 1 Me 30s /rince Methanol	RT	Ni 10 nm

The samples, as received, were loaded into an environmental chamber filled with nitrogen and analysed with an X-ray probe at a wavelength of 0.15406 nm. The final scope is studying interdiffusion and reaction at a fixed temperature after the deposition step as a function of the preparation condition of the silicon surface.

The protocol we applied is depicted in Figure 16, with the temperature raised along the steps and kept for 1 hour at each step. The maximum temperature is intentionally kept below 400 °C.

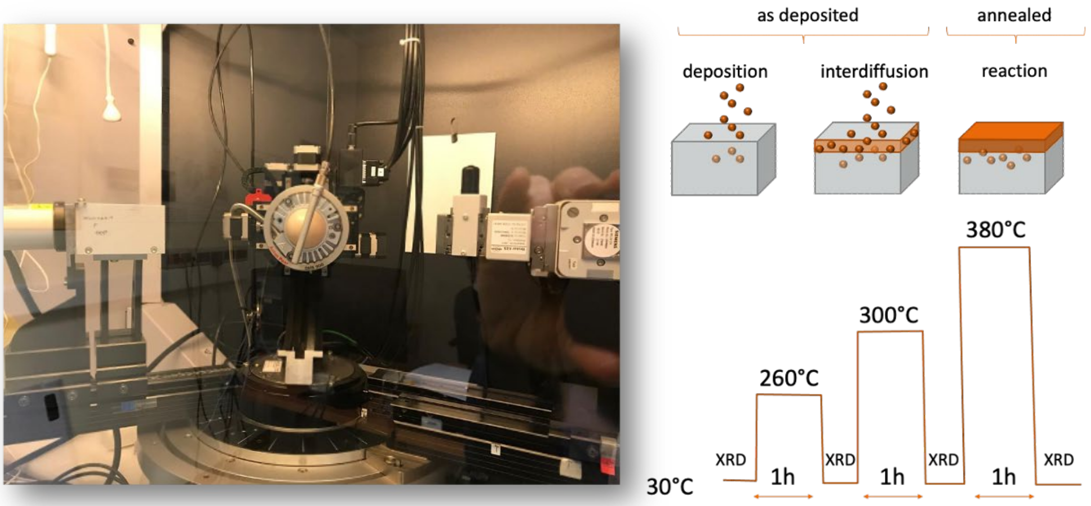

Figure 16. Left panel: X-ray setup with the sample loaded into the environmental chamber located at the center of the equipment; right panel: thermal path to trigger interdiffusion and reaction

After each annealing step, diffraction patterns are collected at the reference temperature of T=30 °C and mutually compared, as shown in Figure 17. The strength of this kind of analysis resides in the *in-situ* investigation done on the same area of the sample that makes the comparison highly reliable on the evolution of the phases.

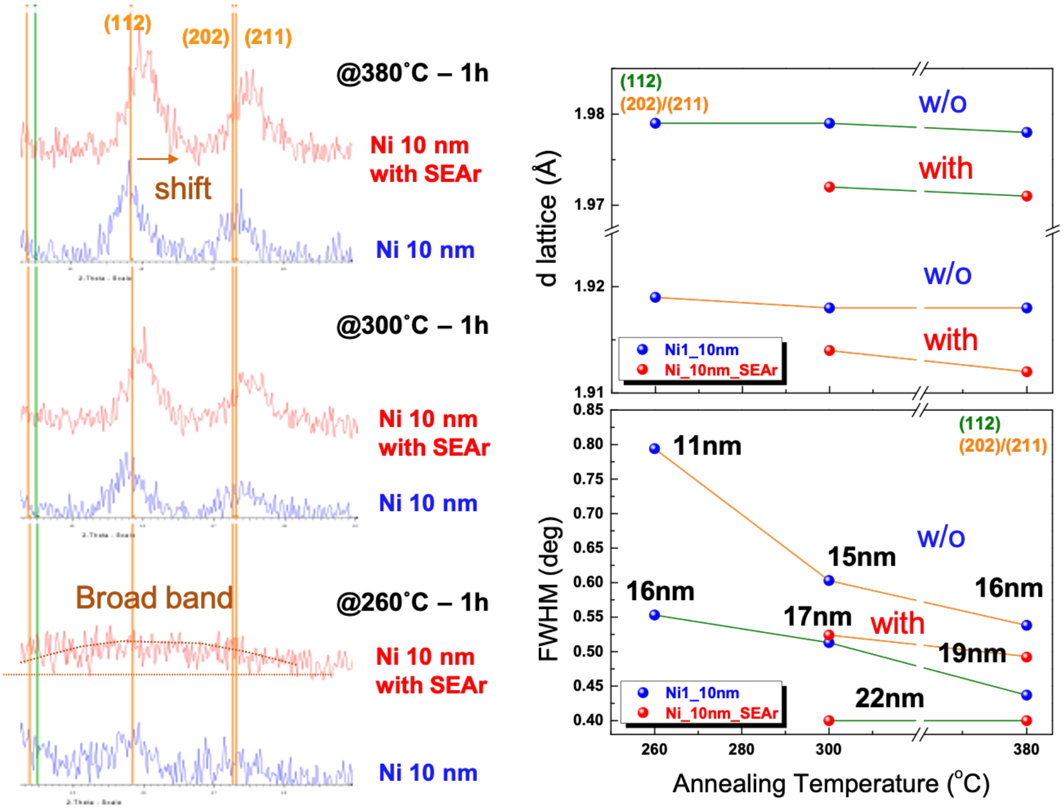

Figure 17 Left panel XRD (grazing incidence) patterns; right panel: data extracted from the XRD patterns, i.e. the interplane lattice distance (d) and Full Width at Half Maximum (FWHM) in the two cases: w/o=without sputter etch; with=with sputter etch applied on silicon before Ni deposition.

As a main evidence after the first annealing step at 260 °C, the nickel layer deposited on the SE-treated surface produces a broad band in the diffraction pattern (Figure 17) that usually characterizes nano-sized or amorphous layers. On the other hand, the diffraction pattern of the sample without SE, after the same thermal budget, has two peaks that indicate the formation of the NiSi phase. By raising the temperature as in the protocol of Figure 16, a progressive increase of the NiSi peak intensity is observed on both samples.

We hereafter summarise further structural differences of the samples w/o vs with SE:

- Larger d-spacing; $\Delta d/d=0.3\text{-}0.4\%$
- Smaller Grain size

In both cases with post-deposition thermal treatments:

- The Grain-size increases with T
- d-spacing slightly reduces with T

The listed differences are symptomatic of interdiffusion and reaction differently occurred in the two samples depending on the surface treatment before nickel deposition. The compositional and structural results hence invite to further investigate the interface status immediately after Ni deposition. The approach used is based on the phase density analysis (Figure 18). Data on the electronic density of the layers are extracted by X-ray Reflectivity profiles and are especially focused towards disentangling eventual differences in the interface composition.

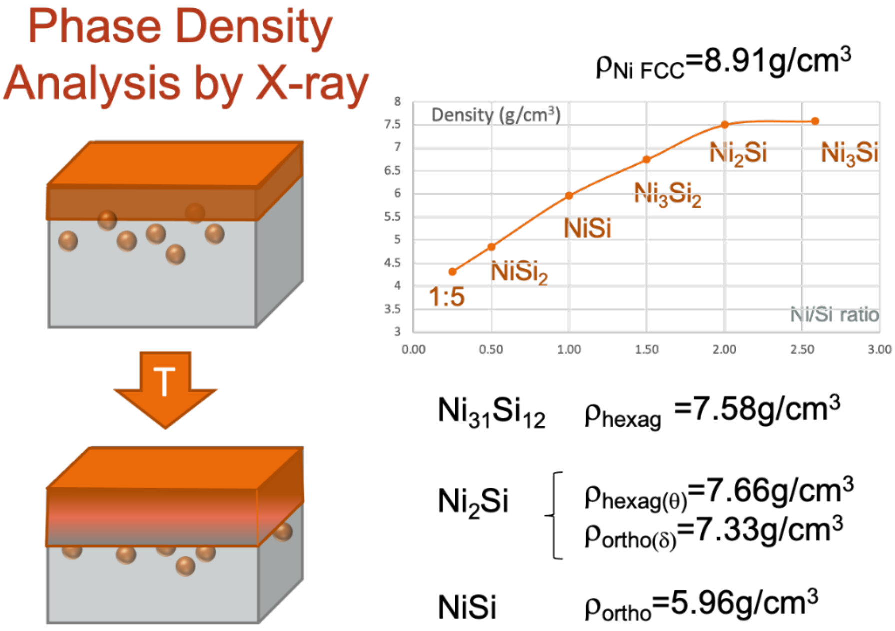

Figure 18. Density vs. composition of the Ni-Si layers as expected by the Phase Density analysis.

It has been found that the sample with SE treatment has an interfacial layer ~3 nm thick located under the pure Nickel layer (10.9 nm thick) whose density is ~3 g/cm^3 indicating a Ni-Si mixing at the interface. Similarly, an interfacial layer is formed without SE, but the density of the layer is higher ~4 g/cm^3. Complementary to this average information, TEM analyses and chemical maps are in progress to go deeper into the atomic profiles.

To summarise, the two methods applied to clean the silicon surface from the native oxide that would inhibit the silicidation process are found to impact on the properties of the reacted layer. In both cases, NiSi is the main phase formed starting form 260 °C, that is a quite low and applicable temperature for devices processing. Nonetheless, difference can be found in the grain size and lattice spacing of the silicide grains, that arises from a different kinetics of Ni-Si mixing since the early deposition step.

Conclusions

In the present document, the initial exploratory activity aiming at the development of atomistic simulation model of the silicides process is presented. In agreement with the plan indicated in the project technical annex these investigations provide a catalogue of configuration/energetic pairs derived by accurate DFT calculations and the initial experimental structural data set (at different stages of the silicidation process) which, when extended further, will be applied for the validation of the simulation predictions. The general consideration emerging from the DFT study is the spontaneous tendency of NiSi system to break the symmetric coherent configurations at the boundaries between phases (see e.g. the panels in Figure 10) to form disordered intermediate states which can be seen as precursors of the formation of a new crystalline phase (i.e. a compound with different stoichiometry and density).

In spite of the completely different character of the study (energetics of static configuration for the DFT analysis, kinetics due to annealing for the real process) the experiments also agree with this scenario: the contact between Ni and Si materials, after the deposition step, leads to the formation of an intermediate strongly disordered layer (quasi-amorphous) which evolves toward the sequence of silicide compounds upon annealing. Moreover, the structure of the final system, and probably the intermediate stage, can strongly depend on the state resulting from the deposition procedure. We notice that experiments have been designed with a fixed protocol of the silicidation and different initial preparation conditions. The in-situ analysis implemented permits to gain access at different reaction stages in a single run. We plan to reproduce this protocol with minor modification in the future experiments, integrating XRD results with other analyses (e.g. TEM or resistance measurements).

The ability to reproduce these aspects seems a crucial feature of the atomistic simulation method and we demonstrate that these findings are in principle accessible to the multi structure LKMC tool under development (see e.g. Figure 12). As discussed, the simulator has not been calibrated yet and the catalogue will be used to achieve an early setting of the parameter used for the determination of the events' rates. Anyhow it appears clear from now that the full functional dependence of these parameters from the local configurations cannot be obtained directly by the DFT energetics due to the plethora of possible atomic arrangements during the kinetics. Although not established in the technical annex, we have also started the derivation of a machine learning semiempirical potential for the Ni-Si system. We strongly believe that, in addition to the new experimental data, the availability of MD simulations based on this potential at finite (high) temperatures (i.e. in a setting which can be also reproduced by the LKMC simulations) will be an important achievement for obtaining a definitive benchmarking and validation of the model.

Bibliography

1. *Inter-diffusion, melting and reaction interplay in Ni/4H-SiC under excimer laser annealing.* **S. Sanzaro, C. Bongiorno, P. Badalà, A. Bassi, G. Franco, P. Vasquez. A. Alberti, A. La Magna.** 2021 , Appl. Surf. Sci., Vol. 539, p. 148218.

2. *Front-end process modeling in silicon.* **L. Pelaz, L.A. Marques, M. Aboy, P. Lopez, and I. Santos.** (2009), Eur. Phys. J. B , Vol. 82, p. 323–359 .

3. *Quantum espresso: a modular and open-source software project for quantum simulations of materials.* **P. Giannozzi, et al.** 2009, J. Phys.: Cond. Matter, Vol. 21, p. 395502.

4. *Generalized gradient approximation made simple.* **J. P. Perdew, K. Burke, and M. Ernzerhof.** 1996, Physical review letters, Vol. 77, p. 3865.

5. *Projector augmented-wave method .* **Blöchl, P.E.** 24, 1994, Physical Review B., Vol. 50, p. 17953–17978.

6. *Finding reaction pathways and transition states: r-artn and d-artn as an efficient and versatile alternative to string approaches.* **A. Jay, C. Huet, N. Salles, M. Gunde, L. Martin-Samos, N. Richard, G. Landa, V. Goiffon, S. De Gironcoli, A. Hémeryck,and N. Mousseau.** 2020, J. Chem. Theory Comput., Vol. 16, p. 6726–6734.

7. *Atomistic calculations of composite interfaces.* **Michael I. Baskes, JE. Angelo, CL Bisson.** 1994, Modelling and Simulation in Materials Science and Engineering, Vol. 23A, p. 505.

8. ***Magali Benoit, et al.*** *2021, Mach. Learn. Sci. Technol. , Vol. 2, p. 025003.*

9. Review paper. ***A.Alberti, A. La Magna.*** *2013, Journal of Applied Physics, Vol. 114, p. 121301.*